Magnetic moments and Pu form factor in $PuFe_2$

M. Wulff, G. H. Lander, J. Rebizant, and J. C. Spirlet
European Institute for Transuranium Elements, Euratom, Postfach 2340 D-7500 Karlsruhe, Germany

B. Lebech and C. Broholm
Physics Department, Risø National Laboratory, Roskilde DK-4000, Denmark

P. J. Brown
Institut Laue-Langevin, 156X, F-38042 Grenoble, France

(Received 8 September 1987; revised manuscript received 16 November 1987)

Neutron diffraction experiments using both polarized and unpolarized beams have been performed on a small (40 mg) single crystal of $^{239}PuFe_2$. This material has the cubic Laves phase structure and is ferromagnetic at ~ 560 K. The polarized-neutron experiments have shown that (a) the easy direction for both the Pu and Fe moments is $\langle 100 \rangle$, (b) the moments are $(0.39 \pm 0.02)\mu_B$ and $(1.73 \pm 0.01)\mu_B$ for the Pu and Fe atoms, respectively, (c) the Fe form factor is the same as in iron metal, and (d) the form factor of Pu is very unusual. The Pu form factor is very different from that found recently in PuSb and cannot be analyzed with a straightforward crystal-field ground state. We suggest that hybridization effects, presumably in the main part between the $3d$ iron and $5f$ plutonium electrons, play a significant role in modifying the spin and orbital contributions that give rise to the unusual Pu form factor.

I. INTRODUCTION

The rare-earth (R) and actinide (A) cubic Laves phase ($C15$ crystal structure) form a very large subset of compounds with many d-electron elements as well as with Al. In the rare-earth systems all the RFe_2 systems order magnetically[1] and the very high T_c's of 600–700 K together with the large magnetocrystalline anisotropy of, for example, the $Dy_xTb_{1-x}Fe_2$ have led to their application in magnetostrictive devices.[2] In the actinide systems, UAl_2 is a spin-fluctuation system,[3] and the Np Laves phases with nonmagnetic d elements show a variety of behavior ranging from localized to itinerant magnetism.[4]

The properties of the AFe_2 compounds as presently found in the literature are given in Table I. The Laves phase structure is shown in Fig. 1. Aldred[5] has measured the magnetic properties by bulk magnetization techniques yielding accurate values for T_c and μ_{eff} (for $T > T_c$), but the values given by him for the total magnetic moment are unreliable because of the large anisotropy in these systems and the lack of single crystals. Lander *et al.*[6] performed neutron diffraction on polycrystalline materials and determined the individual magnetic moments and the easy axes of magnetization. Earlier work with the Mössbauer technique on AFe_2 by Blow[7] and Gal *et al.*[8] had led to contradictions over the easy direction in $PuFe_2$. Both authors agreed that $\langle 111 \rangle$ is the easy direction in UFe_2 and $NpFe_2$ but disagreed over $PuFe_2$. We show in this paper that $\langle 100 \rangle$ is the easy axis in agreement with earlier neutron work.[6]

Although a substantial amount has been done on these systems, new advances in band-structure computations[9] have focused on the role of the $5f$ electrons in the bonding process. In particular, Brooks *et al.*[10] have shown that the $5f$ electrons in UFe_2 hybridize with both the $3d$ Fe electrons and the conduction electrons. Moreover, in an apparent contradiction to our naive picture of orbital moments being associated only with localized states, they

TABLE I. Properties of the AFe_2 compounds as presently known. All have the fcc $C15$ crystal structure. Each A atom is coordinated with 12 Fe atoms at $(11)^{1/2}a_0/8$ and 4 other A atoms at $(3)^{1/2}a_0/4$. Values of T_c and the effective magnetic moment are from Ref. 5. Values of the individual moments in the ordered state were determined by neutron diffraction on polycrystalline samples, Ref. 6.

	a_0 (Å) (300 K)	T_c (K)	μ_{eff} (μ_B/mol)	μ_A (μ_B)	μ_{Fe} (μ_B)	Easy axis
UFe_2	7.058	162(1)	3.03(3)	0.06(1)	0.59(2)	$\langle 111 \rangle$
$NpFe_2$	7.144	492(2)	4.22(2)	1.09(3)	1.35(5)	$\langle 111 \rangle$
$PuFe_2$	7.190	564(2)	3.65(7)	0.45(5)	1.47(5)	$\langle 100 \rangle$
$AmFe_2$	7.300	613(3)	~ 4	$-0.4(1)$	1.7(2)	$\langle 100 \rangle$

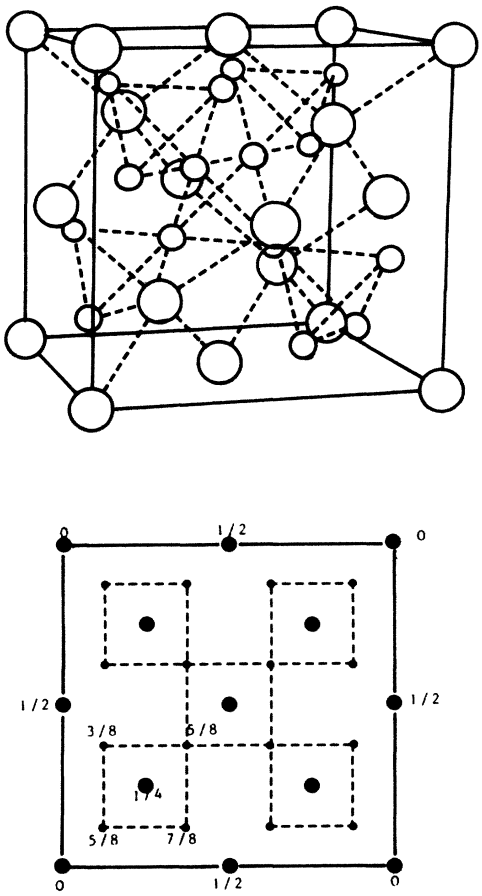

FIG. 1. Laves phase structure of $PuFe_2$. The large circles represent Pu, the small circles are Fe. In the lower figure is shown an [001] projection of the structure with the z parameters marked.

show that large orbital moments are projected out of the hybridized $5f$ states. It is, of course, these orbital moments that couple to the lattice to give the large magnetic-crystalline anisotropies found in both these compounds and the analogous RFe_2 series.[2] Many of these questions posed by theory, as well as a detailed study of the magnetic anisotropy, cannot be answered by experiments on polycrystalline samples. Thus we have instigated a program to grow single crystals of transuranium intermetallics; this paper presents the first report on such single crystals of $PuFe_2$.

II. SAMPLE CHARACTERIZATION

The crystal was grown with the Czochralski technique in a glovebox installation at the European Institute for Transuranium Elements. The starting Pu had the following isotropic composition as of the analysis date of May 1981: 238, 0.06%, 239, 88.95%, 240, 10.17%, 241, 0.70%, 242, 0.11%. ^{241}Pu decays to ^{241}Am with a 13-y half-life but the starting fraction is already small. This is the *same* Pu stock as used to prepare the single crystals of PuSb for unpolarized[11] and polarized-neutron studies.[12] The neutron scattering length of the Pu nucleus in PuSb was found to be 0.800×10^{-12} cm. Correcting for the scattering length[13] of ^{240}Pu of 0.35×10^{-12} cm gives the value of b (^{239}Pu)$=0.850(4)\times10^{-12}$ cm at $\lambda=0.924$ Å. These values are based on a value of b (Sb)$=0.564\times10^{-12}$ and the assumption that the PuSb crystals are stoichiometric, a point about which we have no further details.

As to the impurities in the Pu we know from mass spectroscopy that there are $\sim$4500 ppm Si, and $\sim$1200 ppm of both Al and Na. Other impurities are $\lesssim$100 ppm and the total fraction of magnetic impurities (Gd, Ni, Fe, and Mn) is $\simeq$300 ppm. In addition, the uranium impurities are $\lesssim$100 ppm.

At the time that these crystals were produced we did not have the capability for orienting and cutting them in a glovebox. In fact this proved less of a handicap for the neutron experiments than for bulk measurements. For example, an attempt at Eidgenossiche Technische Hochschule, Zurich[14] to measure the magnetization on three different small crystals gave inconsistent results, and we are unable to present these complementary measurements at this time. A new effort is underway.

Measurements to characterize the crystal quality were made with the sample at room temperature using the four-circle diffractometer at the DR-3 reactor, Risø National Laboratory. The crystal is an irregular piece of weight 40 mg and approximate dimensions of $1\times2\times2.5$ mm.^{3} because of the large absorption of ^{239}Pu ($\sigma=700$ b at 1 Å) the neutron penetration depth is $\sim$0.5 mm so that accurate absorption corrections have to be made for the integrated intensities to be useful, and with an irregular crystal this is difficult. Furthermore, the encapsulation (for security reasons) of the sample with relatively thick-walled aluminum gave rise to strong Al peaks. The presence of these peaks made it necessary to perform ω scans rather than $\omega-2\theta$ scans and use a narrow detector aperture when collecting integrated intensities. As is well known, this leads to a loss of integrated intensity when the Bragg angle θ_B is very different from the monochromator take-off angle θ_M. Because this cutoff function was not measured, it is only possible to compare relative intensities measured within a narrow interval in 2θ.

The contribution to the Bragg intensity from the coherent nuclear scattering is given by

$$I_N(\mathbf{Q})=(8\pi^3/V)N_{\text{cell}}\,|\,N(\mathbf{Q})\,|^2\,,$$

where the structure factor is

$$N(\mathbf{Q})=\sum_j b_j\exp(i\mathbf{Q}\cdot\mathbf{R}_j)e^{-W_j}\,, \tag{1}$$

where the sum is over all the atoms in the unit cell with position $\mathbf{R}_j$ and b and W denote the scattering length and Debye-Waller factor, respectively. V is the volume of the crystal, N_{cell} is the number of cells, and $\mathbf{Q}$ is the scattering vector with $Q=4\pi(\sin\theta)/\lambda$. A direct calculation shows that, when neglecting the Debye-Waller factor, the structure factor falls into six classes, see caption of Table II. The intensity of each class was measured carefully up to $2\theta=90.0°$. Now, by plotting $\ln I_N(\mathbf{Q})$ against Q^2, commonly called the Wilson plot, the reflections fall on six straight lines. Ideally, the slope of each line gives the

TABLE II. Values determined at 4.2 K with polarized neutrons for $PuFe_2$. N is the algebraic expression for $N(\mathbf{Q})$ in Eq. (1) per molecule, γ is determined experimentally, M is determined from Eq. (5) using $b_{Pu}=0.84\times10^{-12}$ and $b_{Fe}=0.954\times10^{-12}$ cm, respectively. We have divided by 0.2695 to give M in effective Bohr magnetons. The product $\mu f(\mathbf{Q})$ for the iron is derived assuming $\mu_{Fe}=1.73(1)\mu_B$ and the Fe elemental form factor. The term $\mu f(\mathbf{Q})$ for the Pu is the quantity of interest; this is plotted in Fig. 4. The N values are $a=b_{Fe}-b_{Pu}/\sqrt{2}$, $b=b_{Pu}$, $c=b_{Fe}+b_{Pu}/\sqrt{2}$, $d=2b_{Fe}$, $e=2b_{Fe}-b_{Pu}$, $f=2b_{Fe}+b_{Pu}$.

hkl	$\frac{\sin\theta}{\lambda}$ (Å^{-1})	N	γ	M (μ_B)	$\lvert\mu f\rvert_{Fe}$ (μ_B)	$\lvert\mu f\rvert_{Pu}$ (μ_B)
111	0.120	a	0.86(2)	1.15	1.492	0.482(4)
220	0.195	b	0.185(1)	0.577		0.577(3)
311	0.229	c	0.256(1)	1.470	1.059	0.58(1)
222	0.239	d	0.281(1)	1.989	1.012	
400	0.276	e	0.287(4)	1.137	0.884	0.631(3)
331	0.301	a	0.270(5)	0.360	0.765	0.57(3)
422	0.338	b	0.203(5)	0.633		0.63(4)
511	0.359	c	0.178(2)	1.022	0.596	0.60(4)
333	0.359	c	0.180(4)	1.034	0.560	0.67(9)
440	0.391	f	0.153(4)	1.560	0.479	0.60(5)
531	0.409	a	0.08(3)	0.107	0.443	0.47(7)
620	0.437	b	0.154(5)	0.480		0.48(2)
533	0.453	c	0.123(6)	0.706	0.322	0.54(5)
622	0.458	d	0.100(2)	0.708	0.343	
444	0.478	e	0.044(8)	0.174	0.262	0.35(8)
642	0.517	b	0.135(9)	0.421		0.42(3)
731	0.530	c	0.083(4)	0.477	0.227	0.35(3)
553	0.530	c	0.102(9)	0.586	0.239	0.49(7)
800	0.552	f	0.077(3)	0.785	0.232	0.32(3)
555	0.598	c	0.05(1)	0.29	0.122	0.24(10)
751	0.598	c	0.066(5)	0.379	0.122	0.36(4)
662	0.602	d	0.0024(5)	0.170	0.105	
844	0.677	f	0.034(3)	0.347	0.047	0.25(3)

temperature factor B_j where $W_j=B_j(\sin^2\theta)/\lambda^2$ and the intercept values give the structure factors and thus a direct check of the stoichiometry of the crystal. The inferred B factors are too high ($2.0\leq B\leq3.0$ Å^2), because the low-angle reflections are magnetically enhanced. However, if we compare the intensities at a high value of Q the magnetic contribution can be neglected. A simple estimate shows that for $Q>4.5$ Å^{-1} the magnetic contribution is less than 2.0% of the nuclear intensity. In Fig. 2 we show a plot of the observed (N_{obs}) versus calculated (N_{calc}) structure factors for reflections near $Q=5$ Å^{-1}. The data points fall on a straight line of slope 1, showing that the stoichiometry is good and that extinction can be ignored.

III. POLARIZED-NEUTRON EXPERIMENTS

A. Instrumental details

The experiments have been performed using the $D3$ polarized-neutron diffractometer at the High-Flux Reactor, Institut Laue-Langevin, Grenoble. The same crystal as examined at Risø was used. The vertical axis of this crystal is close to [013], and this is the applied field direction in the $D3$ instrument. The sample was at 4.2 K in an applied field of 46 kOe. The $D3$ diffractometer employs the normal-beam geometry so that it is possible to examine a large number of reflections with this instrument, not only those in a plane perpendicular to [013].

In analogy with Eq. (1) the magnetic structure factor $\mathbf{M}(\mathbf{Q})$ is given by

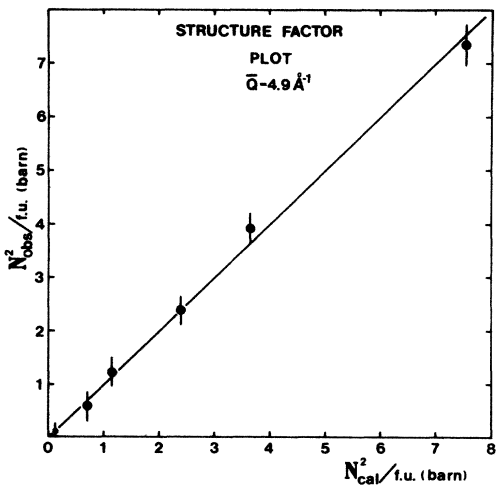

FIG. 2. Results of nuclear intensity measurements with the single crystal. The structure factors N_{obs} and N_{calc} are defined in the text. For an extinction free stoichiometric sample the experimental points should lie on the straight line. $\bar{Q}$ is an average value of Q about which the reflection intensities have been measured. f.u. denotes formula unit.

$$\mathbf{M}(\mathbf{Q})=0.2695\sum_j \mu_j f_j(\mathbf{Q})\exp(i\mathbf{Q}\cdot\mathbf{R}_j)e^{-W_j}\,, \qquad (2)$$

where μ_j is the magnetic moment, $f_j(\mathbf{Q})$ is the associated form factor, and the sum is now over those atoms at positions $\mathbf{R}_j$ which have magnetic moments. The magnetic interaction with the neutron occurs through the vector

$$\mathbf{q}=\hat{\mathbf{Q}}\times(\hat{\boldsymbol{\mu}}\times\hat{\mathbf{Q}}) \qquad (3)$$

in which $\mathbf{Q}$ and $\boldsymbol{\mu}$ are unit vectors in the direction of the scattering vector and magnetic moment, respectively.

In the experiment a beam of polarized monochromatic neutrons is produced from a CoFe crystal. The wavelength used was $\lambda=0.924$ Å. The polarization of the neutrons $\mathbf{P}$ is vertical, i.e., close to the crystal [013] axis, and the polarization efficiency is $|\mathbf{P}|=0.98$. Neutrons can be flipped to a state $-\mathbf{P}$ by a Meissner-Majorana flipper with a 100% efficiency. The experiment consists of measuring the ratio R between the Bragg intensities first with neutrons $+\mathbf{P}$ and then with $-\mathbf{P}$. R is given by

$$R=\frac{N^2+2(\mathbf{P}\cdot\mathbf{q})NM+(\mathbf{q}\cdot\mathbf{q})M^2}{N^2-2(\mathbf{P}\cdot\mathbf{q})NM+(\mathbf{q}\cdot\mathbf{q})M^2}\,, \qquad (4)$$

where we have abbreviated $N(Q)$ to N, etc. We have also taken the vectorial aspect of $\mathbf{M}$ in Eq. (2) and factored out the magnetic moments. As we shall see this is a valid assumption.

Normally in a polarized-beam experiment as performed on $D3$, the magnetization of the sample is parallel to the neutron polarization direction and to the applied field $\mathbf{H}$. In this experiment these conditions are not fulfilled, and it may be asked whether the lack of parallelism between the magnetic moments in the crystal and the applied field has any consequences for the interpretation of the results of the experiment. As a neutron approaches the crystal it is subject to a field which is the sum of the applied field plus that of the magnetic dipole corresponding to the magnetization of the crystal. The dipole field due to a crystal of volume ~ 5 mm^3 with magnetization ~ 20 kOe is very small compared to the applied field of 46 kOe, so the resultant field is about 6° away from $\mathbf{H}$. The neutrons will start to precess about this direction, giving an effective depolarization proportional to the cosine of this angle, which for our purposes can be considered as unity, i.e., a negligible effect. Inside the crystal the magnetic induction with which the neutron interacts is the constant external applied field plus a periodic field due to the magnetized electrons which produces Bragg scattering with a change in spin direction of the scattered neutron. However, so long as there are no regions, such as domain walls, in which the neutron is subject to aperiodic field reversals, there should be no depolarization of the neutron beam.

For the $PuFe_2$ crystal there a number of possible directions for μ_{Pu} and μ_{Fe}. We shall assume both Fe atoms in the asymmetric unit have similar moment directions. Of the many possible arrangements we may select the five cases below:

(a) $\mu_{Pu}\|\mu_{Fe}\|\mathbf{H}$,

(b) $\mu_{Pu}\|\mu_{Fe}\|\langle 100\rangle$,

(c) $\mu_{Pu}\|\mu_{Fe}\|\langle 111\rangle$,

(d) $\mu_{Pu}\|\langle 111\rangle$, $\mu_{Fe}\|\mathbf{H}$,

(e) $\mu_{Pu}\|\langle 100\rangle$, $\mu_{Fe}\|\mathbf{H}$.

Case (a) represents a simple soft magnet, as would be found in transition-metal systems. Case (b) is that proposed by Refs. 6 and 8, case (c) is proposed by Ref. 7, and cases (d) and (e) represent interesting possibilities in which the orbital moment locks the Pu moment in a certain direction, but the iron moment follows the field. Because of strong actinide-iron exchange we would not consider (d) and (e) too likely, but to our knowledge this has not been examined in a microscopic fashion for the analogous rare-earth iron alloys.

B. Directions of magnetic moments

Equation (4) contains explicitly the direction of the moments in the expression for $\mathbf{q}$, Eq. (3), and the interaction with the direction $\mathbf{P}$. Solving Eq. (4) we may obtain an expression for

$$\gamma(\mathbf{Q})=M(\mathbf{Q})/N(\mathbf{Q}) \qquad (5)$$

in terms of the measured flipping ratios $R(\mathbf{Q})$. In each case (a) to (e) above there will be a different relationship between γ and R because these cases correspond to different $\mathbf{q}$ vectors. As an example we may examine the set of $\{220\}$ reflections that have been measured. The $\{220\}$ reflections come *only* from the Pu atoms so they can tell us uniquely the direction of μ_{Pu}, as well as the product $\mu f(Q)$. The six independent reflections are given in Table III. Since there is only one correct value of $\gamma(220)$ we are interested in the internal consistency of the various $\gamma(\mathbf{Q})$ values. The best measure of this is the internal χ^2 calculated from the distribution of values. These χ^2 values range from less than 5 for the [001] direction to absurd values of over 1000 for the [111] and $[\bar{1}11]$ axes, both of which make an angle of 43° with $\mathbf{H}$. Since the [001] is only 18° from $\mathbf{H}$, it is not surprising that $\mu\|\mathbf{H}$ gives a reasonable internal consistency (χ^2 less than 50), but it is still considerably poorer than that with $\mu\|[001]$. We can thus eliminate cases (a), (c), and (e). Similarly we may examine a reflection such as $\{222\}$ for the Fe moment direction, since this has no contribution from Pu. Here we find that $\mu_{Fe}\|[001]$, essentially eliminating all cases except (b).

In concluding this section by confirming cases (b) above, $\mu_{Pu}\|\mu_{Fe}\|\langle 100\rangle$, it is worthwhile pointing out the power of this technique—for example at looking at more complicated ferromagnets or ferrimagnets such as $Nd_2Fe_{14}B$. Depolarization is certainly a potential problem; however, *if* consistency such as shown in Table III is found then depolarization can be neglected. In our case, because of the consistency, depolarization is certainly less than $\sim 5\%$, and probably negligible. It can, of course, be measured directly by looking at the transmitted beam, but with such a small crystal (maximum of 4 mm^2 in

TABLE III. Examination of the {220} and {311} type reflections. $R(\mathbf{Q})$ is the measured flipping ratio, Eq. (4). The final three columns give the derived $\gamma(\mathbf{Q})$ values assuming certain directions from the magnetic moments. The final rows give the weighted mean values and the χ^2 of the distribution. Standard deviations in parenthesis refer to the least significant digit.

h	k	l	N/molecule	R	$\lvert\gamma(001)\rvert$	$\lvert\gamma(-111)\rvert$	$\lvert\gamma(\mathrm{H})\rvert$
2	2	0	b_{Pu}	1.96(1)	0.185(1)	0.234(2)	0.176(1)
2	−2	0		1.95(3)	0.183(7)	0.303(2)	0.174(4)
−2	−2	0		1.97(2)	0.187(7)	0.236(4)	0.177(3)
−2	0	−2		1.42(2)	0.183(2)	0.121(5)	0.160(6)
2	0	−2		1.35(1)	0.17(2)	0.43(2)	0.14(3)
0	2	−2		1.64(2)	0.19(2)	0.17(4)	0.15(4)
			mean		0.185(1)	0.30(11)	0.172(16)
			χ^2		0.3	1614	36
3	−1	1	$1/\sqrt{2}b_{Pu}$	2.56(3)	0.266(3)	0.279(3)	0.240(3)
1	3	−1	$+ b_{Fe}$	2.58(3)	0.253(3)	0.336(4)	0.233(3)
−1	−3	−1		2.02(2)	0.243(4)	0.448(8)	0.263(4)
1	−3	1		2.64(3)	0.261(3)	0.334(7)	0.238(7)
3	1	−1		2.41(2)	0.259(2)	0.358(4)	0.225(2)
−3	−1	−1		2.29(1)	0.256(3)	0.262(3)	0.241(2)
−1	3	−1		2.61(4)	0.253(4)	0.330(5)	0.235(4)
3	−1	−1		2.19(2)	0.254(3)	0.497(6)	0.289(3)
−1	−3	1		2.59(2)	0.253(3)	0.337(3)	0.234(2)
−3	1	−1		2.47(3)	0.256(4)	0.269(3)	0.230(3)
−1	−3	1		2.59(3)	0.253(3)	0.337(3)	0.234(3)
			mean		0.256(1)	0.32(7)	0.239(18)
			χ^2		3	215	39

cross section) this in itself is subject to experimental uncertainties.

C. Determination of magnetic form factors

In the previous section we have identified the magnetic moment direction, now all the data can be processed giving the results in Table II. Although we have in fact least-squared these data to fit the parameters discussed below, it is instructive to discuss a few individual points.

First, there are three reflections (222), (622), and (662) that come from Fe only. The observed values of μf are shown in Fig. 3 as a function of $(\sin\theta)/\lambda$. The solid line, which is the experimentally observed curve of Fe metal,[15,16] is clearly a very good fit to the points. In cubic systems the $3d$ form factors may also show anisotropy due to the T_{2g} or E_g crystal-field configuration. This may be written

$$f(\mathbf{Q})=\langle j_0\rangle+(\tfrac{5}{2}\gamma-1)A_{hkl}\langle j_4\rangle\ , \tag{6}$$

where

$$\langle j_i(Q)\rangle=\int_0^\infty U_{3d}^2(r)j_i(Qr)dr \tag{7}$$

and $U_{3d}^2(\mathbf{r})$ is the radial spin-density distribution of the $3d$ electrons; $j_i(Qr)$ are the spherical Bessel functions. For spherical symmetry $\gamma=0.4$; γ is the parameter giving the occupation of E_g orbitals and in pure Fe is 0.53 ± 0.02. The factor A_{hkl} is a geometric function of

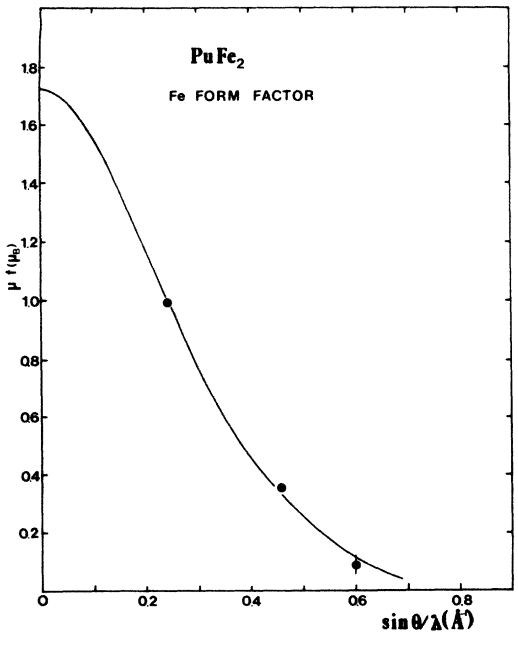

FIG. 3. The solid points are those from reflections with contributions from the Fe atoms only. The solid curve is the elemental Fe form factor fit through the points and giving an iron moment of $1.73\,\mu_B$.

the reflection indices.

We have tried to refine the parameter γ to give either a T_{2g} or E_g occupation but the result is not statistically significant, probably because of our lack of accurate data at high $(\sin\theta)/\lambda$. As a result we have put $\gamma=0.40$, corresponding to a spherically symmetric distribution of $3d$ magnetization density around the Fe nucleus, and used only $\langle j_0\rangle$ as the form factor for iron in $PuFe_2$ (Table II).

To determine $(\mu f)_{Pu}$ we have first the Pu only reflections in Table II; however, to deduce the values we need b_{Pu}. As discussed earlier, we expect $b_{Pu}\simeq 0.80$ based on our work[12] on PuSb, which used the same Pu starting material. With the present set of data we can internally assess the b_{Pu} by minimizing the distribution of $(\mu f)_{Pu}$ about the smooth curve (the theoretical basis for this is given in the next section). On performing this we find $b_{Pu}=0.84(2)$ in $PuFe_2$. Recalling that these values reflect not only scattering lengths, but also stoichiometries, we regard this agreement as satisfactory. Varying b_{Pu} has a negligible effect on the analysis of the Pu form factor, although it is of course correlated with μ_{Pu}.

IV. THE FORM FACTOR OF Pu

A. Experimental analysis

A convenient starting approach for the magnetic form factor of Pu is that found for Pu^{3+} in PuSb.[12] Here we expand Eqs. (6) and (7) to write

$$f_{Pu}(\mathbf{Q})=\langle j_0\rangle+C_2\langle j_2\rangle+C_4\langle j_4\rangle+C_6\langle j_6\rangle\ , \tag{8}$$

where

$$\langle j_i(Q)\rangle=\int_0^\infty U_{5f}^2(r)j_i(Qr)dr \tag{9}$$

with the quantities in Eq. (9) similar to those in (7), except that we must now deal with the radial wave function for the $5f$ electrons, $U_{5f}(r)$. These functions are tabulated by Desclaux and Freeman[17] and have the feature that at $Q=0$, $\langle j_2\rangle=\langle j_4\rangle=\langle j_6\rangle=0$. $\langle j_2\rangle$ has a maximum of 0.21 at $(\sin\theta)/\lambda\simeq 0.35$ Å^{-1} and the other functions have smaller maxima at higher Q values. Although we were able to detect a C_4 value of $\simeq -0.2$ in PuSb (Ref. 12), the present form factor in $PuFe_2$ is not as accurate and we can readily put $C_4=C_6=0$. Since the moment is along [001] the magnetic symmetry is tetragonal and the leading term describing the quadrupole moment has an axial term depending on the angle between the scattering vector $\mathbf{Q}$ and the [001] quantization axis; in spherical harmonic notation this is the angle Θ. The form factor then becomes

$$f(\mathbf{Q})=\langle j_0(Q)\rangle+(C_2+\Delta C_2\sin^2\Theta)\langle j_2(Q)\rangle+\cdots\ . \tag{10}$$

Notice here that the only vectorial dependence of $f(\mathbf{Q})$ is in the term ΔC_2, since $\langle j_i(Q)\rangle$ are functions only of the magnitude of Q.

The shape of the quadrupole distribution (prolate or oblate depending on whether ΔC_2 is less than or greater than zero) is an interesting feature of any Pu form factor,[12] but despite an attempt to analyze this term (by imposing tetragonal symmetry) we do not obtain a statistically significant ΔC_2. The assumed form factor has then a very simple form

$$f(Q)=\langle j_0(Q)\rangle+C_2\langle j_2(Q)\rangle\ , \tag{11}$$

and the *only* parameters are μ, the intercept at $Q=0$, and C_2. Refining these parameters gives

$$\mu_{Pu}=0.39(2)\mu_B\ ,$$

$$C_2=6.0(2)\ .$$

The Pu form factor is shown in Fig. 4.

B. Theoretical considerations

Before continuing with comparisons with other Pu form factors it is useful to consider the form factor from first principles. We shall confine our discussion to the dipole approximation which, like our Eq. (11), involves terms only in $\langle j_0\rangle$ and $\langle j_2\rangle$. Following Marshall and Lovesey[18] we may write for a system in which S, L, and J are good quantum numbers that

$$\mu f(Q)=2\langle S\rangle\langle j_0(Q)\rangle+\langle L\rangle(\langle j_0(Q)\rangle+\langle j_2(Q)\rangle)$$
$$=(2\langle\mathbf{S}\rangle+\langle\mathbf{L}\rangle)\langle j_0(Q)\rangle+\langle\mathbf{L}\rangle\langle j_2(Q)\rangle\ ,$$

since $\mu=2\langle\mathbf{S}\rangle+\langle\mathbf{L}\rangle$, we write

$$f(Q)=\langle j_0(Q)\rangle+\frac{\langle\mathbf{L}\rangle}{2\langle\mathbf{S}\rangle+\langle\mathbf{L}\rangle}\langle j_2(Q)\rangle\ , \tag{12}$$

which must be compared with Eq. (11) to give a definition of C_2. In the case of single-component SLJ states, this gives

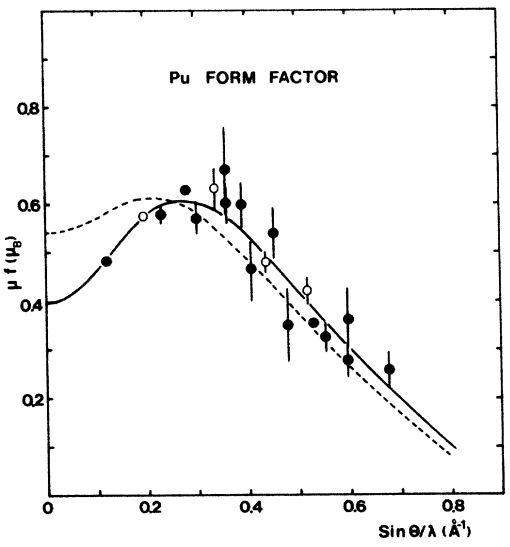

FIG. 4. The experimental points for the Pu form factor in $PuFe_2$. The open circles are those from reflections with contributions from Pu atoms only. The solid circles contain contributions from the Fe site, for which we have used the form factor of Fig. 3. The solid line is a best fit (see text) with $C_2=6.0$ and the dashed line is a best fit using the value of $C_2=3.8$ found in PuSb.

$$C_2=\frac{J(J+1)+L(L+1)-S(S+1)}{3J(J+1)+S(S+2)-L(L+1)} \tag{13}$$

and by algebraic rearrangement we can also show that

$$C_2=\frac{2-g}{g}\ , \tag{14}$$

where g is the Landé splitting factor. It should be remembered that the expressions here are approximations; nevertheless, they show that a large C_2 is associated with a small g and a corresponding cancellation of S and L components. The largest value of C_2 is found in Sm^{3+} compounds,[19] in which the Russell-Saunders coupling scheme with $S=\frac{5}{2}$, $L=5$, and $J=L-S=\frac{5}{2}$ is a good approximation. For Pu^{3+} intermediate coupling[20] mixes in higher-lying S and L states so that the ground state is only $\sim 65\%$ the ^6H state. This leads to an increase in g from $0.286(\frac{2}{7})$ to 0.414 and a corresponding reduction in C_2. The values calculated taking into account all terms in $\langle j_2 \rangle$ are given in Table IV.

To show the difference between the $f(Q)$ for Pu in $PuFe_2$ and PuSb we have performed a least squares on the $PuFe_2$ data with C_2 fixed at its value in PuSb (3.8) and the result is shown as a broken line in Fig. 4. The moment obtained is $0.53\mu_B$. Clearly, this curve fits the data at small $(\sin\theta)/\lambda$ very poorly.

V. DISCUSSION

A. Magnetic anisotropy and Fe form factor

Our measurements show clearly that $\langle 100 \rangle$ is the easy direction of both the Fe and Pu moments in $PuFe_2$. Earlier measurements on polycrystalline samples[5] demonstrated that very large anisotropy exists in these systems. We can safely assume that this arises from the orbital moment of the Pu magnetization and its coupling to the lattice. It would be interesting to study the evolution of the tetragonal distortion and its magnitude at low temperature. A study of this sort was already reported[21] an $NpFe_2$ and $NpNi_2$, both which have $\langle 111 \rangle$ easy axes, and therefore exhibit rhombohedral distortions.

The measurements by Aldred[15] on polycrystalline samples obtain a total moment of $2.3(1)\mu_B$/mol, which is far below the value of $0.39(2)+2\times 1.73(1)=3.85(4)\mu_B$/mol found by the present measurements. Assuming infinite anisotropy about a $\langle 100 \rangle$ axis the magnetization value from a polycrystalline sample with random orientation should be 83.2% of the true value, whereas in this case the relationship is 60%. Even allowing for a 10% conduction-electron polarization leaves an appreciable discrepancy. A possible reason for this discrepancy (suggested to us by the referee) is that the anisotropy freezes the moments along certain cube axes and these do not rotate when a field is applied. The above value of 83.2% assumes, of course, that the moments rotate to the cube direction closest to the applied field, but the anisotropy energy may prevent this. One way to test this would be to cool the sample through T_c in a field, but since T_c is above room temperature (564 K), this is a relatively difficult magnetization experiment with a plutonium sample.

The iron form factor (Fig. 3) is found to be indistinguishable from that of pure Fe. This is not surprising, the iron $3d$ magnetic moment is $1.73(1)\mu_B$ in $PuFe_2$ and $2.2\mu_B$ in Fe metal. The Fe atom in $PuFe_2$ is surrounded by six Fe atoms at 2.54 Å, whereas in bcc Fe there are eight nearest neighbors at $\sqrt{3}a_0/2=2.50$ Å, so the environment is very little changed and the strong Fe-Fe hybridization gives rise to a Fe-like $3d$ band. What is more surprising is that the $3d$ moment on Fe in UFe_2 is so small, see Table I [Yessik[22] obtained values for $0.030(5)\mu_B$ and $0.38(2)\mu_B$ on the uranium and Fe sites, respectively, but Aldred[23] showed that the crystals used by Yessik were nonstoichiometric. Most probably the results in Table I represent those for stoichiometric Laves phases]. Brooks *et al.*[10] have performed band calculations for UFe_2 and show that there is a strong hybridization of the Fe $3d$ and U $5f$ electrons and that the material is only just ferromagnet, with a small Fe moment.

B. Plutonium form factor

In the case of the Pu form factor (Fig. 4) we note that for a large C_2 value (see Table IV) we need a small g value Eq. (14) or, equivalently, a large cancellation between S and L Eq. (14). There are number of ways to arrange this, and we shall first start by looking at the analogous Sm compounds. These have a $4f^5$ configuration and also a small g value. To our knowledge single crystals of $SmFe_2$ have not been examined with polarized neutrons, although it is known that the easy axis is $\langle 111 \rangle$. In addition to Sm metal,[19] results on the compounds $SmAl_2$ (with the Laves phase), $SmCo_5$, and SmZn have been reported.[24] $SmAl_2$ also has $\langle 111 \rangle$ as its easy axis and it can be argued directly from the Steven's factors[2] that because of prolate nature of the charge density for both the Sm^{3+} and Pu^{3+} ions the $\langle 111 \rangle$ each axis would be expected in a cubic Laves compound. Since $PuFe_2$ has a $\langle 100 \rangle$ easy axis, this is the first discrepancy. A similar discrepancy between PuSb, which also has a $\langle 100 \rangle$ easy axis, as compared to SmSb, which has a $\langle 111 \rangle$, has been ascribed by Cooper and his colleagues[25] to anisotropic hybridization effects. No calculations have yet been performed in systems in which strong $3d$ hybridization can be expected, as in $PuFe_2$, so this comparison cannot yet be extended.

TABLE IV. Values of the magnetic moment and the C_2 coefficient for various Pu ground states. Γ_8 and Γ_7 are possible crystal-field states of the ion in a cubic crystal. The experimental value for PuSb is from Ref. 12.

Wave function		Moment (μ_B)	C_2
$J=\frac{5}{2}$	Free ion	1.036	3.80
	Γ_8	0.760	3.62
	Γ_7	0.345	4.48
Experiment	PuSb	0.745±0.020	3.80±0.07
Experiment	$PuFe_2$	0.39±0.02	6.0±0.2

For the Sm compounds the nature of the crystal-field interactions is reasonably well known. For example, in $SmCo_5$ the whole manifold of six states extends over ~ 1200 K in energy. Moreover, since the single-ion, spin-orbit parameter in Sm^{3+} is ~ 1100 cm^{-1} (1580 K) the excited state multiplet ($J=\frac{7}{2}$) lies only ~ 1400 K above the ground state. When the full matrix is diagonalized, including exchange interactions, the ground state includes a small amount (between 4 and 15%) of the $J=\frac{7}{2}$ state. The excited crystal-field states, which can easily be populated at room temperature, contain even more of the $J=\frac{7}{2}$ state, and at higher temperatures in $SmCo_5$ the spin and orbital moments almost cancel. In this case C_2 can be very large. This argument was first presented by de Wijn *et al.*[26] in their attempts to analyze the results of Sm metals. At first glance, therefore, such a large C_2 as we have found in $PuFe_2$ would seem to be explicable with a crystal-field scheme. However, the spin-orbit parameter in Pu^{3+} is twice as big[20] at ~ 2260 cm^{-1} (3250 K) as in Sm^{3+}. The result is that the $J=\frac{7}{2}$ excited state is at ~ 5000 K, and *no* appreciable mixing is possible unless the crystal fields are much bigger than we anticipate from ionic systems.[27] The ground state contains components with different S and L values (this is what we mean by intermediate coupling), but all within the $J=\frac{5}{2}$ manifold. The effect is then to raise g (from $\frac{2}{7}$ to 0.414) and hence reduce C_2 as compared to the Sm^{3+} case. The values in Table IV therefore represent our best expectation for the Pu^{3+} ion and have a maximum value of ~ 4.5. The moment of the Γ_7 state in Table IV is also close to that found in $PuFe_2$, although the easy direction of the Γ_7 doublet is $\langle 111 \rangle$.

The above arguments show that close analogies to the Sm compounds do not exist, despite the similar shape of $f(Q)$. Instead, we believe that the explanation of the large C_2 coefficient must come from a detailed consideration of the hybridization of the electron wave functions that occurs in these actinide intermetallics. The general extent of electron hybridization in actinide intermetallic compounds has been covered recently in a review article by Johansson *et al.*,[28] and Brooks *et al.*[10] have considered the particular case of UFe_2. In none of these cases, however, have the authors projected out the particular expectation values of $\langle S \rangle$ and $\langle L \rangle$, from which a value of C_2 may be estimated by using Eq. (12). Furthermore, a large value of C_2 (of ~ 6) has been reported[29] for the compound UNi_2, which has the hexagonal modification of the Laves phase. In this case the moment is very small ($\sim 0.08\mu_B$) on the U site so the form factor lacks the precision of that we have determined in $PuFe_2$, but the characteristic maximum at $(\sin\theta)/\lambda \sim 0.2$ Å^{-1} is still there.

In conclusion the Pu form factor clearly represents a most sensitive method for examining the electron wavefunction ground state. Whereas in PuSb the $f(Q)$ could be understood with a definite crystal-field ground state,[12] in the case of $PuFe_2$ the situation is more complex. Our results suggest the need to consider a band electron picture, with a strong cancellation of the spin and orbital moments. This is in agreement with general theoretical reviews of these systems, but we lack any definite predictions with which to compare our experimental results.

ACKNOWLEDGMENTS

Discussions with M. Brooks and F. Tasset are gratefully acknowledged. We also wish to thank the Radioprotection Services of the Institute Laue Langevin and Risø National Laboratory for their assistance, during the experiment, and C. Rijkeboer for his help in crystal growth.

[1] K. N. R. Taylor, Adv. Phys. **20**, 551 (1971).
[2] A. E. Clark, in *Handbook on the Physics Chemistry of the Rare Earths,* edited by K. A. Gschneider and L. Eyring (North-Holland, Amsterdam, 1979), Vol. 2, Chap. 15, p. 231.
[3] J. M. van Ruitenbeek, A. P. J. van Deursen, H. W. Myron, A. J. Arko, and J. L. Smith, Phys. Rev. B **34**, 8507 (1986), and references therein.
[4] For a recent review of actinide Laves phases, see J. M. Fournier and R. Troc, in *Handbook of the Physics and Chemistry of the Actinides,* edited by A. J. Freeman and G. H. Lander (North-Holland, Amsterdam, 1985), Vol. 2, p. 29.
[5] A. T. Aldred, J. Magn. Magn. Math. **10**, 53 (1979).
[6] G. H. Lander, A. T. Aldred, B. D. Dunlap, and G. K. Shenoy, Physica **86-88B**, 152 (1977).
[7] S. Blow, J. Phys. C **3**, 835 (1970).
[8] J. Gal, Z. Hadari, E. R. Bauminger, I. Nowik, S. Ofer, and M. Perkal, Phys. Lett. **31A**, 511 (1970).
[9] See, for example, M. S. S. Brooks, B. Johansson, and H. K. Skriver, Ref. 4 (1984), Vol. 1, p. 153.
[10] M. S. S. Brooks, O. Eriksson, and B. Johansson, Phys. Scr. **35**, 52 (1987).
[11] P. Burlet, S. Quezel, J. Rossat-Mignod, J. C. Spirlet, J. Rebizant, W. Müller, and O. Vogt, Phys. Rev. B **30**, 6660 (1984).
[12] G. H. Lander, A. Delapalme, P. J. Brown, J. C. Spirlet, J. Rebizant, and O. Vogt, Phys. Rev. Lett. **53**, 2262 (1985); J. Appl. Phys. **57**, 3748 (1985).
[13] G. H. Lander and M. H. Mueller, Acta Crystallogr. B **27**, 2284 (1971).
[14] O. Vogt and K. Mattenberger (private communication).
[15] C. G. Shull and Y. Yamada, J. Phys. Soc. Jpn. **17**, Suppl, B-III, 1 (1962); C. G. Shull and H. A. Mook, Phys. Rev. Lett. **16**, 184 (1986).
[16] See, for example, H. A. Mook, Phys. Rev. **148**, 495 (1966): W. C. Phillips, *ibid.* **138**, A1649 (1965).
[17] J. P. Desclaux and A. J. Freeman, J. Magn. Magn. Mater. **8**, 126 (1978).
[18] W. Marshall and S. W. Lovesey, *Theory and Thermal Neutron Scattering* (Oxford University Press, Oxford, 1971), p. 152.
[19] W. C. Koehler and R. M. Moon, Phys. Rev. Lett. **29**, 1468 (1972); J. X. Boucherle, D. Givord, and J. Schweizer, J. Phys. (Paris) Colloq. **43**, C7-199 (1983).
[20] W. T. Carnall and B. G. Wybourne, J. Chem. Phys. **40**, 3428 (1964).
[21] M. H. Mueller, G. H. Lander, H. A. Hoff, H. W. Knott, and J.

F. Reddy, J. Phys. (Paris) Colloq. **40**, C4-68 (1979).
[22]M. Yessik, J. Appl. Phys. **40**, 1133 (1969).
[23]A. T. Aldred, J. Magn. Magn. Mater. **10**, 42 (1979).
[24]J. X. Boucherle, D. Givord, J. Laforest, and P. Morin, in *The Rare Earths in Modern Science and Technology,* edited by G. J. McCarthy, J. J. Rhyne, and H. B. Silver (Plenum, New York, 1980), Vol. 2, p. 261.
[25]B. R. Cooper, R. Siemann, D. Yang, P. Thayamballi, and A. Banerjea, Ref. 4, Vol. 2, p. 435.
[26]H. W. de Wijn, A. M. van Diepen, and K. H. J. Buschow, Solid State Commun. **15**, 583 (1974).
[27]S. K. Chan and D. J. Lam, in *The Actinides: Electronic Structure and Related Properties,* edited by A. J. Freeman and J. B. Darby (Academic, New York, 1974), Vol. 1, p. 1.
[28]B. Johansson, O. Ericksson, M. S. S. Brooks, and H. L. Skriver, Phys. Scr. T **13**, 65 (1986).
[29]J. M. Fournier, A. Boeuf, P. Frings, M. Bonnet, J. X. Boucherle, A. Delapalme, and A. Menovsky, J. Less Common Metals **121**, 249 (1986).